Current **A**pplied **S**cience and **T**echnology e-ISSN: 2586-9396

Curr. Appl. Sci. Technol. ….., Vol... (No...), e0266155

Research article

Synthesis and Characterization of Natural HAp/β-TCP Biphasic Calcium Phosphate from Salmon Bone Using a Simplified, Low-cost Technique

Pensri Pramukkul[1], Surirat Yotthuan[2], Aurawan Rittidech[3], Tawat Suriwong[4,5], Theerachai Bongkarn[5,6] and Chittakorn Kornphom[1]*

[1]Department of Physics and General Science, Faculty of Science and Technology, Chiang Mai Rajabhat University, Chiang Mai, 50300, Thailand
[2]Division of Engineering Materials, Department of Science Service, Ratchathewi, Bangkok 10400, Thailand
[3]Department of Physics, Faculty of Science, Mahasarakham University, Mahasarakham, 44150, Thailand
[4]School of Renewable Energy and Smart Grid Technology, Naresuan University, Phitsanulok, 65000, Thailand
[5]Research Center for Academic Excellence in Applied Physics, Faculty of Science, Naresuan University, Phitsanulok, 65000, Thailand
[6]Department of Physics, Faculty of Science, Naresuan University, Phitsanulok, 65000, Thailand

Received: 31 January 2025, Revised: 5 May 2025, Accepted: 5 May 2025, Published: 7 July 2025

Abstract

Bioceramics containing biphasic calcium phosphates (BCP) are the preferred material for various bone healing applications. BCP consists of β-tricalcium phosphate (β-TCP) and hydroxyapatite (HAp) and offers a balance between solubility and resorption, which promotes cell interaction and tissue growth. There is high demand to synthesize BCP from natural sources using simple and inexpensive methods. This study investigated the effects of calcination temperature on the phase structure, chemical composition, and microstructure of BCP powders synthesized from raw salmon bone (Atlantic salmon) using a simplified, low-cost technique. The successful synthesis of BCP powder from raw salmon bone was confirmed using X-ray diffraction (XRD) and Fourier-transform infrared spectroscopy (FTIR). The physical and chemical characteristics were analyzed using scanning electron microscopy (SEM) and energy dispersive spectroscopy (EDS). XRD results revealed the coexistence of HAp and β-TCP phases at calcination temperatures above 600°C for 2 h, indicating the formation of BCP compounds. The relative phase content of HAp and β-TCP changed when the calcination temperature increased from 600 to 1000°C. The crystallite size of HAp and β-TCP increased while the lattice strain decreased as the calcination temperature increased. All samples showed polyhedral lumps of irregular sizes, and the Ca/P ratio decreased from 2.14 to 1.95 with higher calcination temperatures. The FTIR results of all samples revealed the existence of the functional

*Corresponding author: E-mail: Chittakorn_kor@g.cmru.ac.th
https://doi.org/10.55003/cast.2025.266155

groups of phosphate (PO_4^{3-}) hydroxyl (OH^-) and carbonate (CO_3^{2-}), which are characteristic of the BCP structure. The optimal phase ratio of HAp/β-TCP at approximately 60:40 was obtained by the samples at a calcination temperature of 800°C. This study reports on a new simplified, low-cost technique to synthesize BCP powder from salmon bone.

Keywords: biphasic calcium phosphate; bioceramic; calcination; fish bone; a simplified; low-cost technique

1. Introduction

The primary composition of human teeth and bone consists of calcium and phosphate, accounting for approximately 70% of the structure (Abdulridha et al., 2024). Teeth and bone are the second most commonly implanted tissues in the human body, following blood. Over the years, teeth and bone graft scaffolds have become essential in treating, repairing, and augmenting skeletal injuries, functioning as bone replacement materials (Venkatesan & Kim, 2014). Bioceramics composed of calcium and phosphate are widely valued for their chemical compatibility and bioactivity, making them useful for regenerating and replacing human teeth and bones (Gallant et al., 2014). However, bioceramics are expensive because they require costly precursor chemicals or complex synthetic processes (Shi et al., 2018). Additionally, concerns about bioactivity and the potential for rejection within the human body present serious concerns when developing substitute materials (Gallant et al., 2014; Shi et al., 2018).

Biphasic calcium phosphate (BCP) is a biomaterial composed of two phases: hydroxyapatite [$Ca_{10}(PO_4)_6(OH)_2$; HAp)] and β-tricalcium phosphate [$Ca_3(PO_4)_2$; β-TCP]. BCP has recently garnered interest as a scaffolding material. The chemical composition of BCP is similar to the mineral component of human bone, with a molar Ca/P ratio near 1.67, and its solubility promotes biomineralization around bone implants (Ebrahimi et al., 2017; Ahmadi et al., 2022; Deng et al., 2022a; 2022b). BCP is less hydrophobic than β -TCP but more hydrophobic than HAp (Wang et al., 2012). Compared to HAp, BCP demonstrates better osteopromotion because of its hydrophobic interactions, which promote protein adsorption (Wang et al., 2012). In addition to encouraging efficient bone ingrowth, this property ensures good stability (Suneelkumar et al., 2008; Cheng et al., 2010; Ebrahimi et al., 2017). To address bone deformities in high-load-bearing locations, BCP materials can be tailored to maintain their shape over extended periods (de Oliveira et al., 2007) by appropriately modifying the phase concentrations. Additionally, BCP can be consolidated by controlling the degree of Ca deficiency in the initially formed non-stoichiometric apatite and optimizing the conditions of subsequent firing (Duta et al., 2021). BCP can be produced through both natural and chemical methods, although chemical synthesis involves complex processes that require chemical reagents (Zhang et al., 2013; Chen et al., 2015; Malakausaite-Petruleviciene et al., 2015; Iyyappan et al., 2016; Othman et al., 2016; Duta et al., 2021). Moreover, various chemical routes to synthesize BCP powders have been developed, such as wet chemical precipitation, hydrothermal reaction, mechanochemical–hydrothermal synthesis, and sol–gel synthesis (Duta et al., 2021). On the other hand, there are a few drawbacks to these approaches. One of them is that it may be challenging to keep the pH value over 9 in the initial solution using these methods (Duta et al., 2021). Another is that they produce calcium-deficient BCP powders, which quickly break down to β-TCP when heated further. It is well established that HAp and β-TCP are the primary constituents of natural bones, such as those from fish, bovine, and pig sources. Fish bones are rich in calcium, carbonate, and phosphate compounds, making them a reliable source

for producing BCP from natural materials (Duta et al., 2021). Moreover, the HAp and β-TCP derived from fish sources exhibit thermal stability at higher temperatures (Duta et al., 2021).

Increasing global fish consumption has led to the generation of significant amounts of fish bone waste annually. Globally, approximately 970-2700 billion tons of fish are harvested, of which humans consume 450-1000 billion tons, with nearly 50% of the total being wasted (Muhammad et al., 2017; Shi et al., 2018, Duta et al., 2021;). This has led to interest in utilizing fish bone waste as a resource for sustainable BCP production. Recent studies have synthesized BCP from the fish bones of various species, including Sheelavati (roho labio) fish (Sunil et al., 2016), tuna fish (Latif et al., 2020), milkfish (Lolo et al., 2022), Tylosurus crocodilus (Permatasari et al., 2020) and butterfish (Deng et al., 2022a), each employing distinct synthesis processes. Larosi et al. (2009) reported simplified procedures for extracting BCP powders from several kinds of fish. One approach involves calcining the fish bones at 950°C for 12 h and then crushing the resulting powder for 1 min in a ball mill. Another approach combined laser irradiation with calcination treatment (200-400°C). This method of obtaining powders from fish bones was much quicker than the traditional calcination one, thanks to the high energy density of the laser (Larosi et al., 2009). Moreover, BCP with HAp/β-TCP ratios of 50/50 or 60/40 significantly enhanced cell proliferation (Kong et al., 2008; Ahmadi et al., 2022). BCP powder with HAp/β-TCP ratios of 64/36 was successfully synthesized with salmon bones using the calcination process (Zhu et al., 2017). This process used a calcination temperature of 1000°C for 1 h with a heating rate of 5°C/min in air and then cooling at 20°C/min to room temperature (Zhu et al., 2017). In recent years, salmon bone has gained interest as a promising material for synthesizing high-quality HAp powder due to its availability and low cost (Komur et al., 2017; Tri et al., 2020; Nguyen et al., 2022). However, researchers are attempting to resolve the ongoing issues in developing BCP bioceramics with a high concentration of β-TCP components using an easy and practical approach.

This study aimed to synthesize BCP powder with HAp/β-TCP ratios of 60/40 from salmon bone using a simplified and low-cost technique. The bone was heat-treated using an air fryer and ground by hand milling before the calcination process. The effect of calcination temperature on salmon bone's chemical composition, structural formation, and microstructure was studied.

2. Materials and Methods

Raw salmon bones (Atlantic salmon) obtained from the salmon processing industry were boiled in water at 100°C for 2 h to remove any remaining flesh. To eliminate proteins, lipids, and other organic contaminants, the cleaned salmon bones were treated with 1% NaOH in acetone for 24 h and then rinsed with pure water. The cleaned bones were dried and heat-treated at 200°C for 30 min using an air fryer. The dried and crisped salmon bones were ground by hand milling for 20 min using a mortar and then sieved through a 200-mesh screen. The resulting salmon bone powder was calcined at temperatures ranging from 600 to 1000°C for 2 h in air with a heating rate of 5^{o}C/min and allowed to cool down naturally. This procedure was repeated 3 times. The synthesis process of biphasic calcium phosphates from salmon bone powder is summarized schematically in Figure 1.

Figure 1. Schematic diagram of the synthesis process for biphasic calcium phosphates from salmon bone powders using a simplified, low-cost technique

The thermal transformations during the calcination of salmon bone powders were analyzed using a TG-DSC analyzer (NETZSCH, STA 449 F3). Thermogravimetric analysis (TG) and differential scanning calorimeter (DSC) were performed on the powders over a temperature range of 40°C to 1000°C at a heating rate of 10°C/min. The crystal structure of calcined salmon bone powders at room temperature, prepared at various calcination temperatures, was determined using X-ray diffraction (XRD, Rigaku, SmartLab) with Cu-Kα radiation (λ = 1.5418 Å). XRD data were recorded over a 2θ range of 10-80° with a scanning rate of 0.05°/s. The phase formation was identified by comparing experimental XRD patterns with standard data from the Joint Committee on Powder Diffraction Standards (JCPDS) files No. 09-0432 and No.09-0169. The microstructure of all samples was examined using field-emission scanning electron microscopy (FE-SEM; Thermoscientific Model, Apreo S). Chemical compositions were analyzed using energy dispersive spectroscopy (EDS). Samples were prepared for SEM analysis by mounting them on conductive adhesive and supported on conventional carbon microgrids. The chemical functional groups of all samples were analyzed using Fourier-transform infrared spectroscopy (Perkin Elmer, Frontier) in transmission mode, with wavelengths ranging from 450 to 4000 cm^{-1}.

3. Results and Discussion

Figure 2 displays the TG and DSC results of salmon bone powders being calcined over a temperature range of 40-1000°C. The TG and DSC curves revealed three distinct decomposition zones (Figure 2). In the first zone (I) at around 40-150°C, the TG curve exhibited a weight loss of 4.15%, attributed to the elimination of incorporated water, which was supported by an endothermic peak in the DSC curve at approximately 150°C as seen in Figure 2. The second zone (II) (150-520°C) exhibited a rapid weight loss of 28.67% in the TG curve, corresponding to the removal of organic components such as protein and

collagen (Figure 2). This decomposition corresponded to the exothermic peaks in the DSC curve at 341°C and 421°C. In the third zone (III), at around 520-800°C, the TG curve indicated slight changes with total weight loss reaching 33.73% as observed in Figure 2. A small, broad DSC peak around 690°C suggested the decomposition of certain mineral phases. The formation of HAp/β-TCP phases likely occurred at temperatures above 690°C, as the %weight stabilized. The TG results revealed a total weight loss of approximately 33.73% across the temperature range of 40-1000°C, indicating that the final BCP content was approximately 66.27% of the initial material. The TG and DSC results of the salmon bone powders in this work are similar to those previously reported (Onishi et al., 2008, Naga et al., 2015)

The raw Atlantic salmon bones were investigated by X-ray diffraction (XRD), as shown in Figure 3 (a). The XRD pattern revealed the major XRD peak of monocrystalline apatite in the bone matrix, which matched the HAp pattern in the data standard JCPDS No. 09-0432. The crystalline phase of the BCP powders calcined from salmon bones was analyzed using XRD at room temperature, as shown in Figure 3 (b). At a calcined temperature of 600°C, the XRD patterns exhibited broader peaks, and some characteristic hydroxyapatite (HAp) phase peaks (indexed as •) were observed. In contrast, peaks for beta-tricalcium phosphate (β-TCP) did not appear (Figure 3 (b)). This suggests that organic matter in the salmon bone matrix was not completely eliminated, based on the data standard JCPDS No. 09-0432 (Figure 3 (b)) (Rajesh et al., 2012). When calcination temperatures increased from 700 to 1000°C, the XRD peaks became sharper, and the peaks corresponding to the HAp structure were clearly observable, indicating a rise in crystallinity. Additionally, the β-TCP phase (indexed as ♦) emerged at higher calcination temperatures, and the peaks became more defined and aligned with the JCPDS standard data (No. 09-0169). These results demonstrate that calcination temperatures above 700°C can produce BCP powders because the XRD pattern revealed the coexisting HAp and β-TCP phases, corresponding with the TG-DSC data.

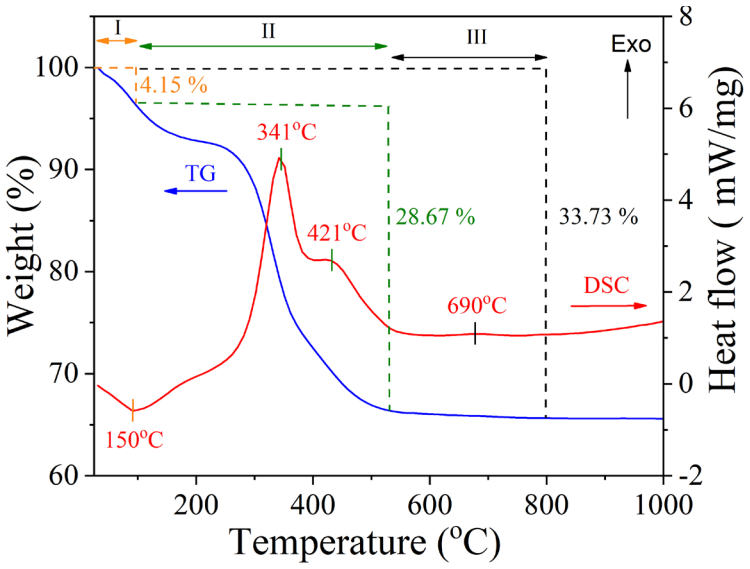

Figure 2. TG and DSC curves of salmon bone powder calcined over a temperature range of 40-1000°C

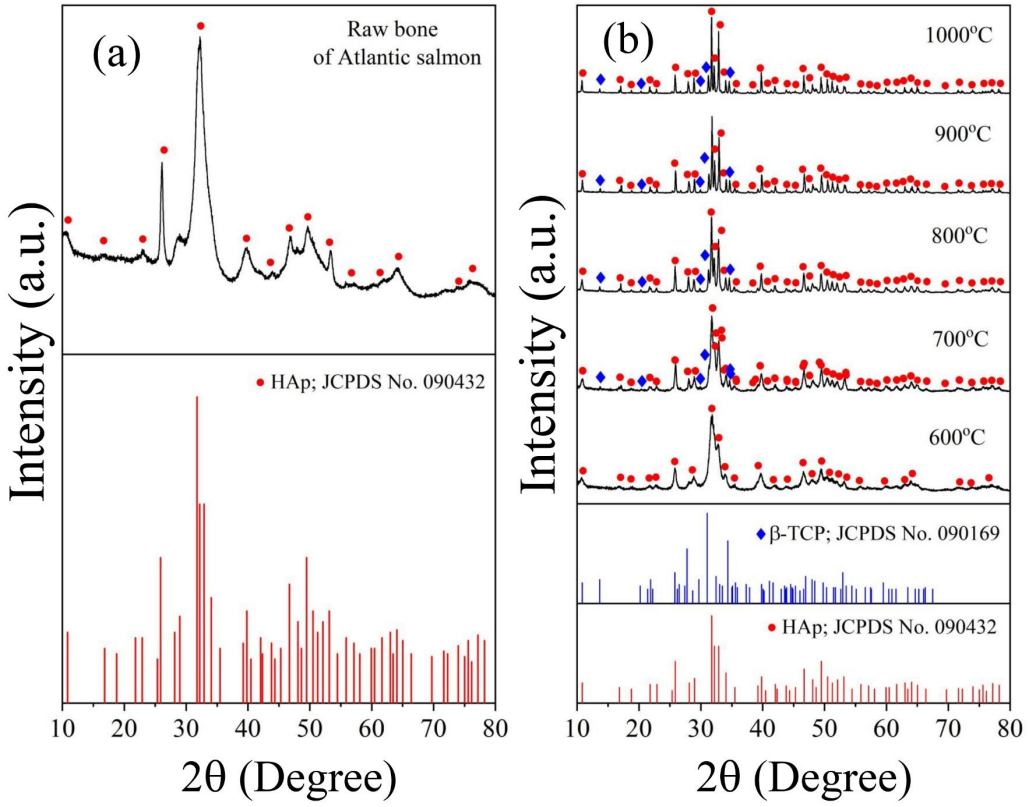

Figure 3. XRD patternd of (a) Atlantic salmon raw bone and (b) salmon bones calcined with temperature from 600 to 1000°C for 2 h

The weight percentages of the HAp phase ($\%\ W_{HAp}$) and β-TCP phase ($\%\ W_{\beta-TCP}$) in the calcined powders were calculated using equations (1) and (2) (Deng et al., 2022b).

$$\%\ W_{HAp} = \frac{I_{HAp}}{I_{HAp} + \frac{I_{\beta-TCP}}{K_{HAp}^{\beta-TCP}}} \times 100 \quad (1)$$

$$\%\ W_{\beta-TCP} = \frac{I_{\beta-TCP}}{I_{\beta-TCP} + I_{HAp} K_{HAp}^{\beta-TCP}} \times 100 \quad (2)$$

Where I_{HAp} represents the intensity of the maximum diffraction peak of the HAp crystal (the (211) plane at 2θ around 31.77°), and $I_{\beta-TCP}$ represents the intensity of the maximum diffraction peak of the β-TCP crystal (the (0210) plane at 2θ around 31.02°). The intensities were derived from XRD data of calcined powders at 800-1000°C, where the peaks for the HAp and β-TCP phases were clearly distinguishable. The analysis revealed that as the calcination temperature increased from 800 to 1000°C, the $\%W_{HAp}$ increased from 65.65 to 80.65%, while the $\%W_{\beta-TCP}$ decreased from 35.35 to 19.35%, as summarized in Table 1.

Table 1. % W_{HAp}, % $W_{\beta\text{-}T}$, crystallite size, and lattice strain of HAp and β-TCP synthesized from salmon bone at various calcination temperatures

Calcination Temperatures (°C)	% W_{HAp}	% $W_{\beta\text{-}TCP}$	The Crystallite Size of HAp (Å)	The Crystallite Size of β-TCP (Å)	Lattice Strain of HAp (%)	Lattice Strain of β-TCP (%)
700	-	-	350	-	0.362	-
800	65.65	35.35	466	432	0.271	0.276
900	79.88	20.12	526	524	0.241	0.246
1000	80.65	19.35	843	525	0.151	0.245

The crystallite size and lattice strain of HAp and β-TCP in the calcined powders were calculated using equations (3) and (4), respectively (Bhardwaj et al., 2023).

$$D = \frac{k\,\lambda}{\beta\cos\theta} \tag{3}$$

$$B_r\cos\theta = \frac{k\lambda}{D} + \varepsilon\sin\theta \tag{4}$$

Where D represents the crystallite size, k is Scherer's constant (0.89), λ is the X-ray wavelength, β is the full width at half-maximum (FWHM) of the (211) peak for HAp and the (0210) peak for β-TCP, θ is the diffraction angle in radians, B_r is the broadening of the diffraction peak (FWHM in radians), and ε is the stress distribution within the material. The lattice strain (ε) was determined using the linear relationship between $B_r\cos\theta/\lambda$ and $\sin\theta/\lambda$, according to the Hall–Williamson principle (Bhardwaj et al. 2023). The calculated crystallite size (D) and lattice strain of HAp and β-TCP for all calcined powders are listed in Table 1. It was observed that the crystalline sizes of the HAp and the β-TCP increased with rising calcination temperature, while the lattice strain decreased. The larger crystallite size with higher calcination temperatures can be attributed to the elimination of imperfections and abnormalities during heat treatment, leading to a well-defined crystalline phase (Saikumari et al. 2021). Conversely, the decrease in lattice strain is affected by the larger crystallites, which reduce atomic configuration changes in nanoregions and eliminate numerous defects within the lattice structure, resulting in decreased lattice strain (Bhardwaj et al., 2023).

To confirm the phase percentages of the HAp and β-TCP phases, the Rietveld method was used to evaluate the XRD patterns and determine the phase content of each calcined powder. In the Rietveld refinement process, the crystal symmetry of the space group P63/m of the HAp phase (COD file no. 1011242) and the R3c:H of the β-TCP phase (COD file no. 1517238) was analyzed using a Pseudo Voigt peak shape function for all diffraction patterns. The atomic positions were treated as variable parameters. Throughout the refinement process, lattice parameters, cation occupancies, isothermal parameters, peak shape parameters, and scale factors were designated as free parameters. The background was also refined via the Pseudo Voigt function. Several factors, including crystallite size, cation arrangement, and electron density, were subsequently specified by refinement, resulting in an optimal value of chi-square (χ^2). Furthermore, analysis of structural bonding was carried out based on the results of the Rietveld refinement (Kornphom et al. 2023; 2024). The refinement results for each calcined powder are presented in Figures 4 (a)-(c), and the refinement parameters are in Table 2. In Figures 4

(a)-(c), the experimental data are represented by red circles, while the simulated data are shown as black lines. The solid blue line represents the difference between the calculated and experimental plots, and the vertical green bars represent the Bragg reflections for the selected space groups of R3c:H and P63/m (Figures 4 (a)-(c)). It is widely accepted that R_{wp}^2/R_{exp}^2 and χ^2values below 4 indicate good agreement between the fits and the data (Kornphom et al., 2024). The R_{wp}^2/R_{exp}^2 and χ^2 values in this work were ≤ 2.65 and $\chi^2 \leq$ 2.65, respectively, demonstrating good fits for all samples, as seen in Table 1. The refinement results confirmed the presence of mixed β-TCP and HAp phases in all samples. The % phase of β-TCP increased from 11 to 40%, while the % phase of HAp decreased from 89 to 60% when the calcination temperature increased from 600 to 800°C (Table 2). However, at calcination temperatures above 800°C, the phase trend reversed, and the amount of β-TCP decreased. The phases percentages found from the refinement results are close to the weight percentages found using equations (1) and (2). Previous research reported that BCP with HAp/β-TCP ratios of 50/50 or 60/40 significantly enhanced cell proliferation (Kong et al., 2008; Ahmadi et al., 2022). In this work, the sample calcined at 800°C exhibited an HAp/β-TCP phase ratio of approximately 60/40, highlighting its potential for biomedical applications.

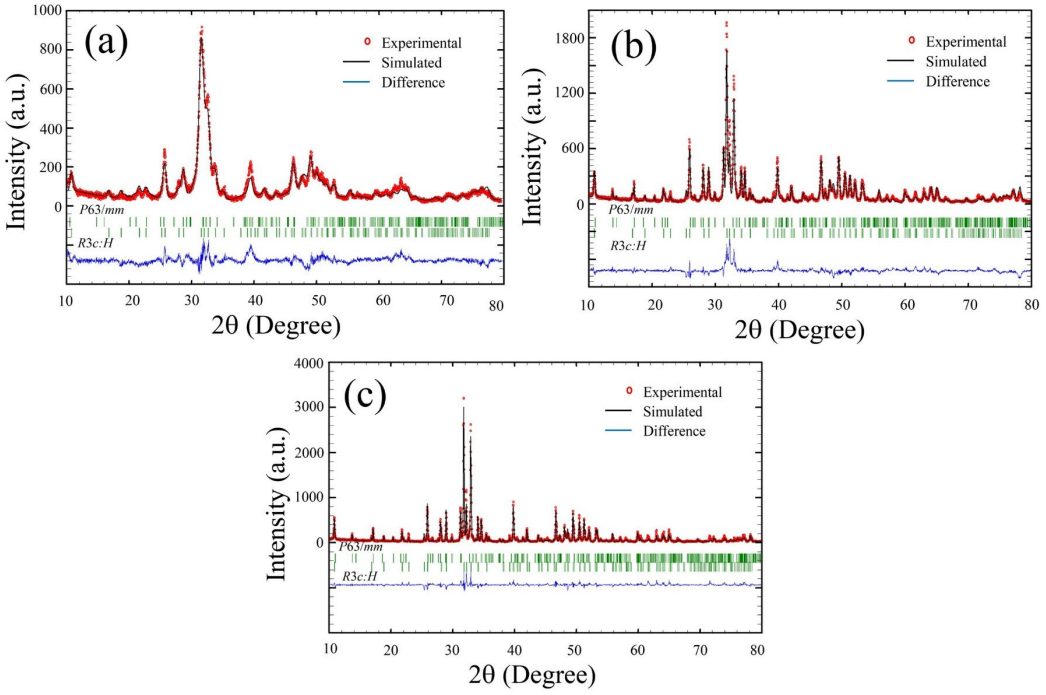

Figure 4. Rietveld refinement results of samples calcined at temperatures of (a) 600°C, (b) 800°C, and (c) 1000°C for 2 h

Table 2. Refinement parameters and phase percentages of HAp and β-TCP in calcined salmon bone powders produced with various temperatures

Calcination Temperatures	Refinement Parameters	Phase Structures	Profile Parameters	Atom Information					The Percentage of Phase
				Label	*x*	*y*	*z*	Occ.	
600°C	χ^2=2.65	β-TCP	*a*= 7.0726Å	Ca1	0.7259	0.8618	0.1663	0.59363	11
	R_p=31.6%	*R* 3 *c* :*H*	*c*= 50.6757Å	Ca2	0.6188	0.8255	-0.0332	0.68149	
	R_{wp}=32.8%		*u*= 84.2187	Ca3	0.7266	0.8514	0.0611	0.55214	
	R_{exp}=20.13%		*v*= 9.57050	Ca4	0.0000	0.0000	-0.0851	0.65353	
	R_{wp}^2/R_{exp}^2=2.65		*w*= -3.4666	Ca5	0.0000	0.0000	0.7336	0.48645	
				P1	0.0000	0.0000	0.0000	0.50193	
				P2	0.6872	0.8606	0.8685	0.95768	
				P3	0.6530	0.8464	0.7668	0.43555	
				O1	0.7256	-0.0944	-0.0917	1.23050	
				O2	0.7674	0.7833	0.8548	1.06014	
				O3	0.7298	0.0088	0.8486	1.08407	
				O4	0.5221	0.7608	0.8627	1.18374	
				O5	0.5987	-0.0488	0.7794	1.02568	
				O6	0.5738	0.6930	0.7850	0.95472	
				O7	0.0803	0.8990	0.7771	0.99183	
				O8	0.6320	0.8258	0.7268	1.13171	
				O9	0.0057	0.8624	-0.0115	1.03531	
				O10	0.0000	0.0000	0.0421	0.99849	
		HAp *P63/m*	*a*= 9.5014Å	Ca1	0.3333	0.6667	0.0000	0.86708	89
			c= 6.9259Å	Ca2	0.2500	0.0000	0.2500	1.00863	
			u= -0.8552	P1	0.4170	0.3610	0.2500	1.12709	
			v= 1.2185	O1	0.3330	0.5000	0.2500	1.17241	
			w= 0.1326	O2	0.6000	0.4670	0.2500	0.99872	
				O3	0.3330	0.2500	0.0630	1.24120	
				O4	0.0000	0.0000	0.2500	0.96713	
700°C	χ^2=3.00	β-TCP	*a*=6.7788Å	Ca1	0.7259	0.8618	0.1663	0.73254	35
	R_p=24.3%	*R* 3 *c* :*H*	*c*=50.3978Å	Ca2	0.6188	0.8255	-0.0332	0.77967	
	R_{wp}=29.2%		*u*=17.1934	Ca3	0.7266	0.8514	0.0611	0.59894	
	R_{exp}=16.22%		*v*=6.6225	Ca4	0.0000	0.0000	-0.0851	0.62649	
	R_{wp}^2/R_{exp}^2=3.22		*w*=1.9762	Ca5	0.0000	0.0000	0.7336	0.58849	
				P1	0.0000	0.0000	0.0000	0.19259	
				P2	0.6872	0.8606	0.8685	0.64491	
				P3	0.6530	0.8464	0.7668	0.53283	
				O1	0.7256	-0.0944	-0.0917	0.83552	
				O2	0.7674	0.7833	0.8548	1.06014	
				O3	0.7298	0.0088	0.8486	1.08407	
				O4	0.5221	0.7608	0.8627	1.18374	
				O5	0.5987	-0.0488	0.7794	1.02568	
				O6	0.5738	0.6930	0.7850	0.95472	
				O7	0.0803	0.8990	0.7771	0.99183	
				O8	0.6320	0.8258	0.7268	1.12522	
				O9	0.0057	0.8624	-0.0115	1.03531	
				O10	0.0000	0.0000	0.0421	0.99849	
		HAp *P63/m*	*a*=9.4531Å	Ca1	0.3333	0.6667	0.0000	0.82652	65
			c=6.8922Å	Ca2	0.2500	0.0000	0.2500	0.96319	
			u=-0.2907	P1	0.4170	0.3610	0.2500	0.95287	
			v=0.5878	O1	0.3330	0.5000	0.2500	1.01605	
			w=0.0024	O2	0.6000	0.4670	0.2500	0.99872	
				O3	0.3330	0.2500	0.0630	1.64355	
				O4	0.0000	0.0000	0.2500	0.96713	

Table 2. Refinement parameters and phase percentages of HAp and β-TCP in calcined salmon bone powders produced with various temperatures (continued)

Calcination Temperatures	Refinement Parameters	Phase Structures	Profile Parameters	Atom Information					The Percentage of Phase
				Label	*x*	*y*	*z*	Occ.	
800°C	χ^2=3.83	β-TCP	*a*=10.3503Å	Ca1	0.7259	0.8618	0.1663	1.10002	40
	R_p=24.9%	*R* 3 *c* :*H*	*c*=37.0992Å	Ca2	0.6188	0.8255	-0.0332	1.01006	
	R_{wp}=29.4%		*u*=0.2779	Ca3	0.7266	0.8514	0.0611	1.14601	
	R_{exp}=15.00%		*v*=0.0030	Ca4	0.0000	0.0000	-0.0851	0.19726	
	R_{wp}^2/R_{exp}^2=3.84		*w*=37.0992	Ca5	0.0000	0.0000	0.7336	0.29203	
				P1	0.0000	0.0000	0.0000	0.25913	
				P2	0.6872	0.8606	0.8685	0.83218	
				P3	0.6530	0.8464	0.7668	1.16063	
				O1	0.7256	-0.0944	-0.0917	1.12727	
				O2	0.7674	0.7833	0.8548	1.27731	
				O3	0.7298	0.0088	0.8486	1.03580	
				O4	0.5221	0.7608	0.8627	1.12282	
				O5	0.5987	-0.0488	0.7794	1.56812	
				O6	0.5738	0.6930	0.7850	0.92978	
				O7	0.0803	0.8990	0.7771	0.87641	
				O8	0.6320	0.8258	0.7268	0.88162	
				O9	0.0057	0.8624	-0.0115	1.04578	
				O10	0.0000	0.0000	0.0421	0.52432	
		HAp *P63/m*	*a*=9.4221Å	Ca1	0.3333	0.6667	0.0000	0.69253	60
			c=6.8814Å	Ca2	0.2500	0.0000	0.2500	0.86187	
			u=0.0414	P1	0.4170	0.3610	0.2500	1.01969	
			v=-0.0045	O1	0.3330	0.5000	0.2500	1.09772	
			w=0.0457	O2	0.6000	0.4670	0.2500	0.77899	
				O3	0.3330	0.2500	0.0630	1.57032	
				O4	0.0000	0.0000	0.2500	0.59084	
900°C	χ^2=3.16	β-TCP	*a*=10.3569Å	Ca1	0.7259	0.8618	0.1663	1.05651	29
	R_p=17.1%	*R* 3 *c* :*H*	*c*=37.1215Å	Ca2	0.6188	0.8255	-0.0332	1.11065	
	R_{wp}=21.5%		*u*=0.1196	Ca3	0.7266	0.8514	0.0611	0.94146	
	R_{exp}=12.09%		*v*=-0.0159	Ca4	0.0000	0.0000	-0.0851	0.23923	
	R_{wp}^2/R_{exp}^2=3.18		*w*=0.0141	Ca5	0.0000	0.0000	0.7336	0.31207	
				P1	0.0000	0.0000	0.0000	0.33556	
				P2	0.6872	0.8606	0.8685	1.20882	
				P3	0.6530	0.8464	0.7668	1.15913	
				O1	0.7256	-0.0944	-0.0917	1.12727	
				O2	0.7674	0.7833	0.8548	0.43889	
				O3	0.7298	0.0088	0.8486	0.79484	
				O4	0.5221	0.7608	0.8627	1.25091	
				O5	0.5987	-0.0488	0.7794	1.73015	
				O6	0.5738	0.6930	0.7850	1.01840	
				O7	0.0803	0.8990	0.7771	0.41085	
				O8	0.6320	0.8258	0.7268	0.97681	
				O9	0.0057	0.8624	-0.0115	1.55044	
				O10	0.0000	0.0000	0.0421	0.41758	
		HAp *P63/m*	*a*=9.4245Å	Ca1	0.3333	0.6667	0.0000	0.69476	71
			c=6.8840Å	Ca2	0.2500	0.0000	0.2500	0.84036	
			u=0.0272	P1	0.4170	0.3610	0.2500	1.01466	
			v=-0.0059	O1	0.3330	0.5000	0.2500	1.13982	
			w=0.0144	O2	0.6000	0.4670	0.2500	0.75105	
				O3	0.3330	0.2500	0.0630	1.61349	
				O4	0.0000	0.0000	0.2500	0.60321	

Table 2. Refinement parameters and phase percentages of HAp and β-TCP in calcined salmon bone powders produced with various temperatures (continued)

Calcination Temperatures	Refinement Parameters	Phase Structures	Profile Parameters	Atom Information					The Percentage of Phase
				Label	*x*	*y*	*z*	Occ.	
1000ºC	χ^2=2.99	β-TCP	*a*=10.3629Å	Ca1	0.7259	0.8618	0.1663	0.99410	20
	R_p=19.3%	*R* 3 *c* :*H*	*c*=37.1488Å	Ca2	0.6188	0.8255	-0.0332	1.12582	
	R_{wp}=24.2%		*u*=0.1279	Ca3	0.7266	0.8514	0.0611	0.91730	
	R_{exp}=14.02%		*v*=-0.0291	Ca4	0.0000	0.0000	-0.0851	0.25558	
	R_{wp}^2/R_{exp}^2=2.98		*w*=0.0132	Ca5	0.0000	0.0000	0.7336	0.21733	
				P1	0.0000	0.0000	0.0000	0.35579	
				P2	0.6872	0.8606	0.8685	0.76850	
				P3	0.6530	0.8464	0.7668	1.29235	
				O1	0.7256	-0.0944	-0.0917	1.20420	
				O2	0.7674	0.7833	0.8548	1.26885	
				O3	0.7298	0.0088	0.8486	1.09856	
				O4	0.5221	0.7608	0.8627	0.63754	
				O5	0.5987	-0.0488	0.7794	0.67983	
				O6	0.5738	0.6930	0.7850	1.22429	
				O7	0.0803	0.8990	0.7771	0.74656	
				O8	0.6320	0.8258	0.7268	1.19240	
				O9	0.0057	0.8624	-0.0115	0.61246	
				O10	0.0000	0.0000	0.0421	0.85913	
		HAp *P63/m*	*a*=9.424739Å	Ca1	0.3333	0.6667	0.0000	0.60956	80
			c=6.884093Å	Ca2	0.2500	0.0000	0.2500	0.79743	
			u=0.077038	P1	0.4170	0.3610	0.2500	0.92481	
			v=-0.049849	O1	0.3330	0.5000	0.2500	1.11017	
			w=0.018359	O2	0.6000	0.4670	0.2500	0.73011	
				O3	0.3330	0.2500	0.0630	1.33323	
				O4	0.0000	0.0000	0.2500	0.56379	

Figures 5 (a) and (b) show the EDS mapping results for the elemental distribution in salmon bone powder calcined at 800°C for 2 h. The mapping revealed a uniform distribution of Ca, P, O, and C across the surface, which confirmed the homogeneous composition of the calcined sample. The microstructure of salmon bone powders calcined with various temperatures exhibited polyhedral lumps of irregular sizes, as seen in Figures 6 (a)(I)-(e)(V). These shapes resulted from all samples being hand-milled into powders before the calcining process. The distribution and average grain size are shown in the inset in Figures 6 (a)(I)-(e)(V). The average particle size of all samples was measured from an SEM image using the Image J program. It was found that average grain size increased from 64.72 to 122.52 μm when the calcination temperature increased from 600 to 1000°C. High calcination temperatures can cause an increase in crystallite size and particle size due to the growth, agglomeration, or fusion of individual domains of particles (Berent et al. 2019). The change in the grain size distribution was insignificant with increasing calcination temperature, which may be caused by hand milling creating non-uniform particle sizes before the calcination process (inset of Figures 6 (a)(I)-(e)(V)).

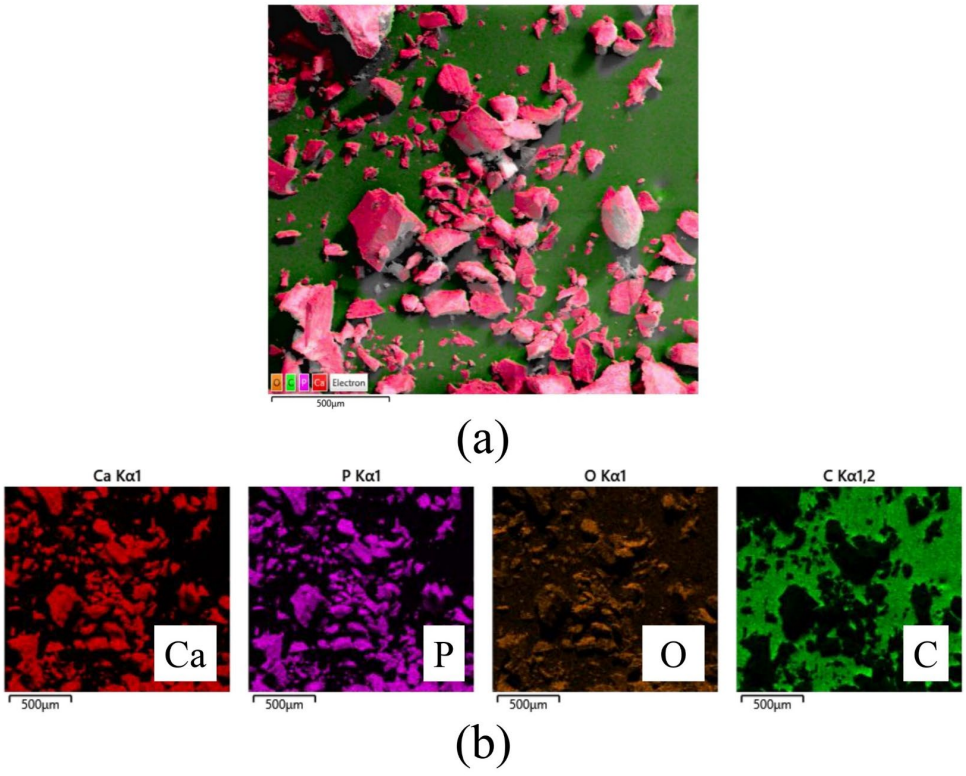

Figure 5. EDS mapping of surface elemental distribution of the powder calcined at 800°C for 2 h (a) combined elements and (b) individual elements of Ca, P, O, and C

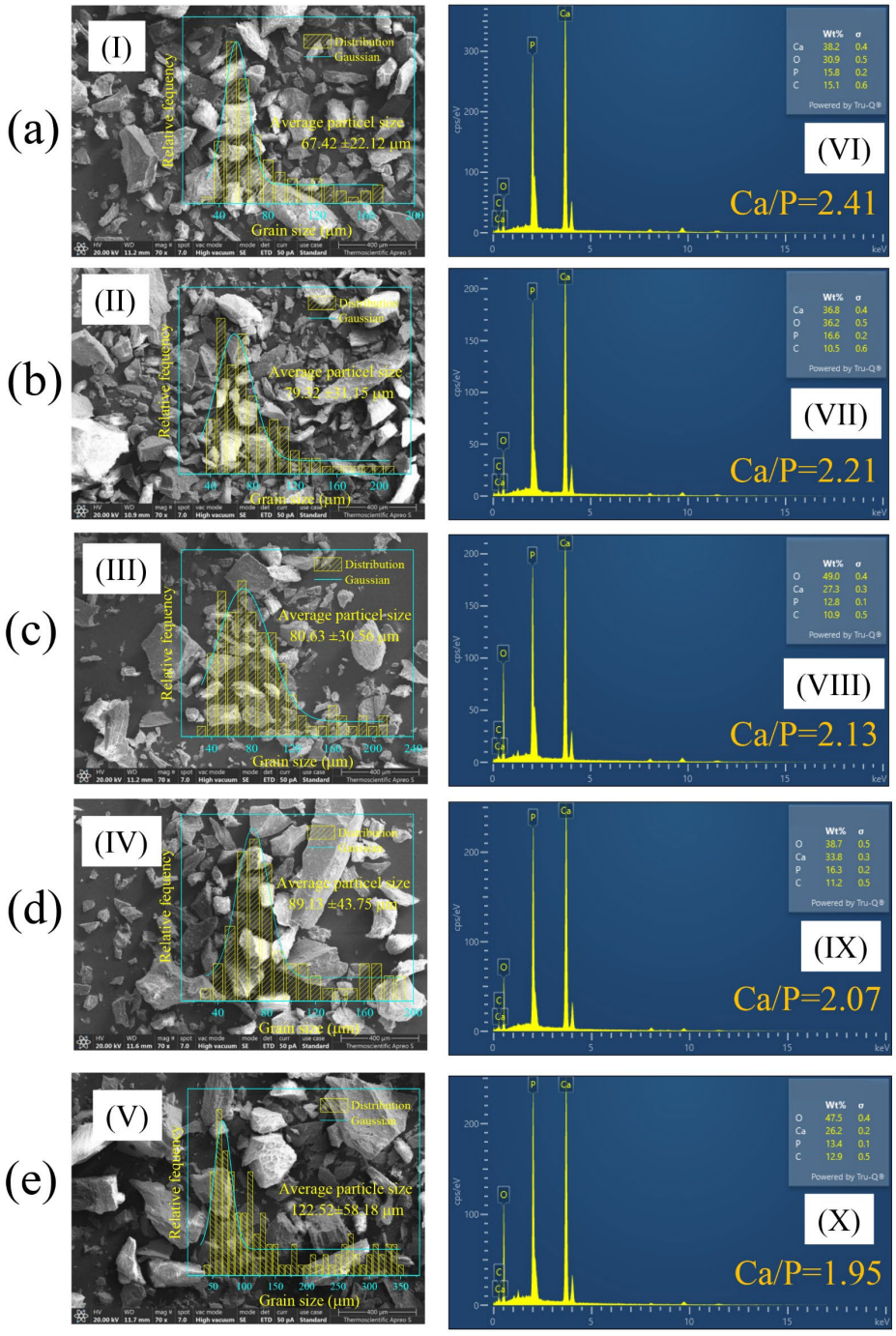

Figure 6. SEM images with the distribution and average grain size and EDS analysis of salmon bone powders calcined at (a) 600°C, (b) 700°C, (c) 800°C, (d) 900°C, and (e) 1000°C for 2 h

The elemental distribution and Ca/P ratios of the calcined samples were determined using EDS, as shown in Figures 5 (a)(VI)-(e)(X). The EDS results revealed high amounts of Ca, P, and O, with small amounts of C. The unspecified spectra is the Au electrode coating. The Ca/P chemical ratio decreased from 2.41 to 1.95 as the calcination temperature increased from 600 to 1000°C for 2 h, as seen in Figures 6 (a)(VI)-(e)(X). The Ca/P ratio in this study was higher than the previous stoichiometric value of HAp (1.67) (Afriani et al. 2020), likely due to HAp breaking down into β-TCP and other phases as the Ca component was lost during the calcination process, which was consistent with the reaction described by equation (5) (Kostov-Kytin et al. 2018). The EDS results corresponded with the XRD results, confirming the formation of the HAp and β-TCP phases. These phases were uniformly dispersed in the calcined samples, resulting in the production of the BCP compound.

$$Ca_{10-x}(HPO_4)_x(PO_4)_{6-x}(OH)_{2-x} \rightarrow Ca_{10}(PO_4)_2 + \beta - Ca_3(PO_4)_2 + xH_2O \quad (5)$$

Fourier transform infrared spectroscopy (FTIR) is crucial for the chemical characterization of predominant functional groups. This method is applicable for the chemical examination of BCP and other organic constituents. BCP consists of phosphate (PO_4^{3-}) hydroxyl (OH^-) and carbonate (CO_3^{2-}) groups which exhibit characteristic infrared (IR) vibrations in the range between 400 and 4000 cm^{-1} (Koutsopoulos et al., 2002). Generally, the PO_4^{3-} group exhibits characteristic IR absorption bands, with bending vibrations of P-O groups around 565-573 cm^{-1} and 602-603 cm^{-1}, and stretching vibrations at 960-962 cm^{-1}, 1040-1050 cm^{-1}, and 1089-1090 cm^{-1}. For the OH group, the stretching vibrations of O-H bonds produce characteristic IR peaks near 632-635 cm^{-1} and 3570-3572 cm^{-1} (Liou et al., 2004; Xu et al., 2004; Motskin et al., 2009). The CO_3^{2-} groups show characteristic stretching deformation bands of C=O bonds between 1400 and 1500 cm^{-1} and around 875 cm^{-1}, respectively (Truite et al., 2022).

In this work, the FT-IR results of samples calcined at various temperatures are shown in Figures 7 (a)-(e), and the frequency range of characteristic IR spectra in all samples are summarized in Table 3. It was observed that the FT-IR curve of all samples showed the PO_4^{3-} peak with bending bands in the range of 559-565 cm^{-1} and 598-600 cm^{-1}, respectively, as well as PO_4^{3-} bands with stretching vibrations in the range of 962-963 cm^{-1}, 1011-1030 cm^{-1}, and 1086-1087 cm^{-1}, as seen in Figures 7 (a)-(e) and Table 3. The OH^- peak with stretching vibrations in the range of 629-632 cm^{-1} and 3571-3573 cm^{-1} was seen in all samples (Figures 7 (a)-(e) and Table 3). The CO_3^{2-} peaks were observed around 879 cm^{-1} and 1457 cm^{-1} for the sample calcined at 600°C (Figure 7 (a) and Table 3), while the samples calcined at 700-1000°C, showed only the CO_3^2 peak at 1457 cm^{-1} (Figures 7 (b)-(e) and Table 3). The FT-IR results in this work confirmed that the samples had typical chemical groups of BCT, consistent with previous work (Koutsopoulos et al., 2002; Shi et al., 2018). Therefore, a BCP powder with an optimal HAp:β-TCP ratio of 60:40 can be synthesized from salmon bone using a simplified, low-cost technique with a calcination temperature of 800°C, with a calcination temperature lower than in previous studies (Larosi et al., 2009; Zhu et al., 2017).

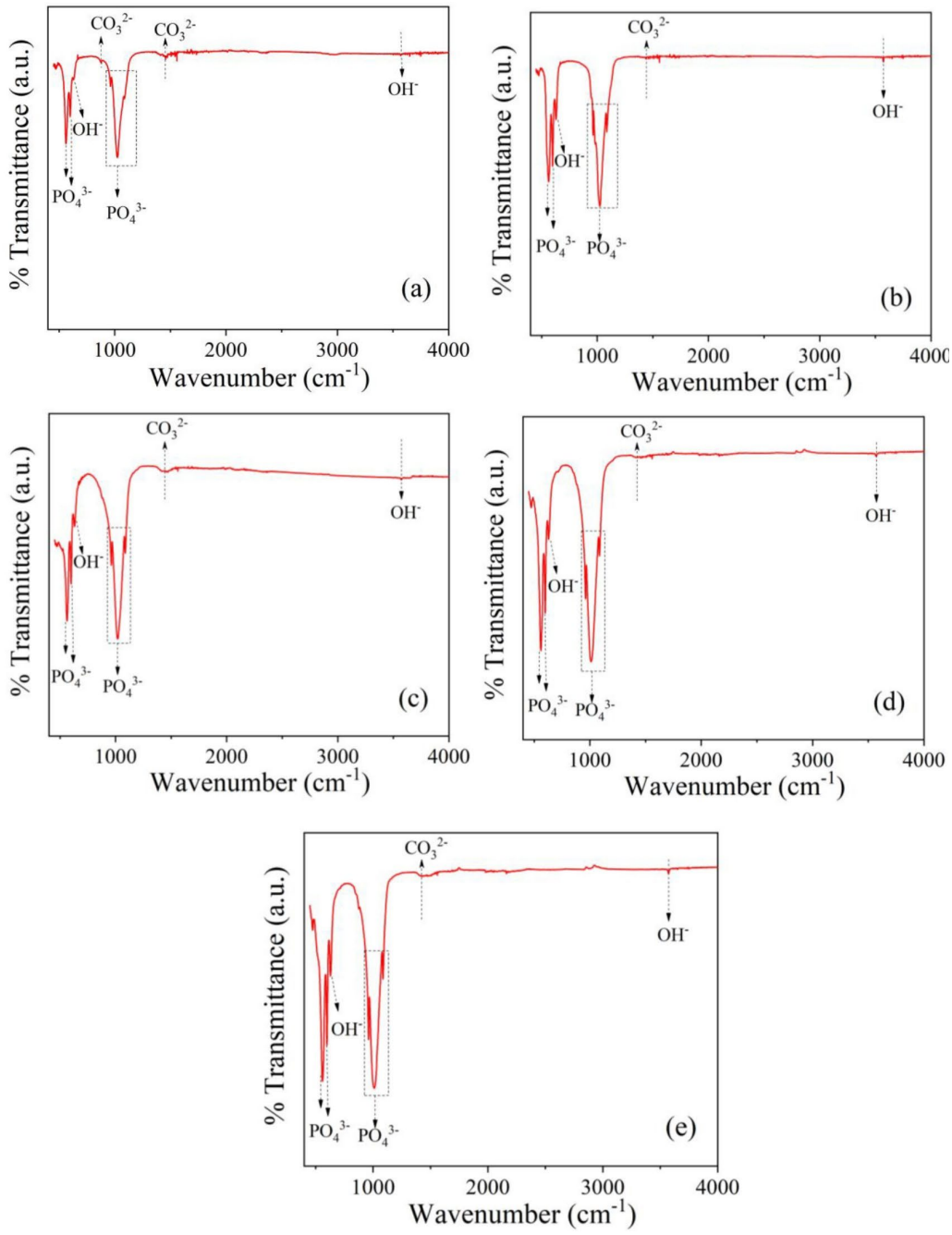

Figure 7. FT-IR spectra of calcined powders at temperatures of (a) 600°C, (b) 700°C, (c) 800°C, (d) 900°C, and (e) 1000°C for 2 h

Table 3. Characteristic IR peaks in the FT-IR spectra of calcined salmon bone powders at various temperatures

Calcination Temperatures (°C)	Characteristic IR Frequency Range (cm^{-1})			
	PO_4^{3-}	OH^-	PO_4^{3-}	CO_3^{2-}
600	562, 600	630, 3571	962, 1024, 1087	879, 1457
700	563, 599	630, 3573	963, 1024, 1087	1457
800	565, 600	632, 3571	963, 1030, 1087	1457
900	560, 599	630, 3571	962, 1011, 1086	1457
1000	559, 598	629, 3572	962, 1011, 1086	1437

4. Conclusions

BCP powder was successfully synthesized from raw salmon bone using a simplified and low-cost technique. The effects of calcination temperature on the phase structure, microstructure, and chemical composition of the samples were studied. Samples calcined at temperatures above 600°C exhibited mixed HAp and β-TCP phases. As the calcination temperature increased, the phase proportions of HAp and β-TCP, as well as the Ca/P ratios, were influenced by the decomposition of the Ca component during the calcination process. The FTIR spectra in all samples confirmed the formation of phosphate (PO_4^{3-}) hydroxyl (OH^-) and carbonate (CO_3^{2-}), which are characteristic of the BCP structure. The sample calcined at 800°C was identified as the most suitable BCP compound due to its nearly equal phase ratio of HAp to β-TCP (60/40). These findings suggest that the BCP synthesized in this study holds promise as a biomaterial for bone replacement applications in the future. However, the synthesized crystalline powder needs to be further studies in depth, for biocompatibility and mechanical properties.

5. Acknowledgements

This work was financially supported by the research fund of Chiang Mai Rajabhat University, Grant number 27/2568 and Naresuan University and the National Science, Research, and Innovation Fund (NSRF), Grant No. R2568B001. The authors wish to thank the Department of Physics, Faculty of Science, Naresuan University, and the Department of Physics and General Science, Faculty of Science and Technology, Chiang Mai Rajabhat University for their supporting facilities. Thanks, are also given to Asst. Prof. Dr. Kyle V. Lopin for his help in editing the manuscript.

6. Authors' Contributions

Pensri Pramukkul: Methodology, Validation, Formal analysis, Writing - Original draft, and Writing- Review & Editing. Surirat Yotthuan: Investigation, Resources. Aurawan Rittidech: Investigation, Resources. Tawat Suriwong: Investigation, Resources. Theerachai Bongkarn: Writing - Original Draft and Writing - Review & Editing. Chittakorn Kornphom: Conceptualization, Methodology, Validation, Formal analysis, Investigation, Writing - Original Draft and Writing - Review & Editing.

7. Conflicts of Interest

The authors and the institutes where the work has been carried out declare that there are no conflicts of interest regarding the publication of this article.

ORCID
Chittakorn Kornphom https://orcid.org/0000-0003-1028-4791
Theerachai Bongkarn https://orcid.org/0000-0001-5321-430X
Surirat Yotthuan https://orcid.org/0000-0003-3848-7566
Aurawan Rittidech https://orcid.org/0000-0002-6734-6490
Tawat Suriwong https://orcid.org/0000-0002-8674-622X

References

Abdulridha, N. J., Al-Ghaban, A. M., & Al-Obaidi, A. J. (2024). Physical and structural properties of biphasic calcium phosphate BCP reinforced with silicene fillers. *AIP Conference Proceedings,* 3091(1), Article 030003. https://doi.org/10.1063/5.0204640

Afriani, F., Siswoyo, Amelia, R., Hudatwi, M., Zaitun, & Tiandho, Y. (2020). Hydroxyapatite from natural sources: methods and its characteristics. *IOP Conference Series: Earth and Environmental Science*, 599, Article 012055. https://doi.org/10.1088/1755-1315/599/1/012055

Ahmadi, M., Dini, G., Afshar, M., & Ahmadpour, F. (2022). Synthesis, characterization, and bioactivity evaluation of biphasic calcium phosphate nanopowder containing 5.0 mol% strontium, 0.6 mol% magnesium, and 0.2 mol% silicon for bone regeneration. *Journal of Materials Research*, 37(11), 1917-1928. https://doi.org/10.1557/s43578-022-00604-3

Berent, K., Komarek, S., Lach, R., & Pyda, W. (2019). The effect of calcination temperature on the structure and performance of nanocrystalline mayenite powders. *Materials*, 12(21), Article 3476. https://doi.org/10.3390/ma12213476

Bhardwaj, S., Thakur, N., & Kumar, S., (2023). Effect of calcination temperature on structural and electrical properties of $K_{0.5}Bi_{0.5}TiO_3$ ceramics prepared by solid-state route. *Bulletin of Materials Science*, 46, Article 170. https://doi.org/10.1007/s12034-023-03014-1

Chen, J., Wen, Z., Zhong, S., Wang, Z., Wu, J., & Zhang, Q. (2015). Synthesis of hydroxyapatite nanorods from abalone shells via hydrothermal solid-state conversion. *Materials and Design,* 87, 445-449. https://doi.org/10.1016/j.matdes.2015.08.056

Cheng, L., Ye, F., Yang, R., Lu, X., Shi, Y., Li, L., Fan, H., & Bu, H. (2010). Osteoinduction of hydroxyapatite/beta-tricalcium phosphate bioceramics in mice with a fractured fibula. *Acta Biomaterialia*, 6(4), 1569-1574. https://doi.org/10.1016/j.actbio.2009.10.050

de Oliveira, R. S., Brigato, R., Madureira, J. F. G., Cruz, A. A. V., Filho, F. V. D. M., Alonso, N., Machado, H.R. (2007). Reconstruction of a large complex skull defect in a child: a case report and literature review. *Child's Nervous System*, 23(10), 1097-1102. https://doi.org/10.1007/s00381-007-0413-7

Deng, K., Chen, H., Dou, W., Cai, Q., Wang, X., Wang, S., & Wang, D. (2022a). Preparation and characterization of porous HA/β- TCP biphasic calcium phosphate derived from butterfish bone. *Materials Technology*, 37(10), 1388-1396. https://doi.org/10.1080/10667857.2021.1950886

Deng, K., Liu, Z., Dou, W., Cai, Q., Ma, W., & Wang, S. (2022b). HA/β-TCP biphasic calcium phosphate ceramics derived from butterfish bones loaded with bone marrow mesenchymal stem cells promote osteogenesis. *Frontiers in Materials*, 9, Article 928075. https://doi.org/10.3389/fmats.2022.928075

Duta, L., Dorcioman, G., & Grumezescu, V. (2021). A review on biphasic calcium phosphate materials derived from fish discards. *Nanomaterials*, 11(11), Article 2856. https://doi.org/10.3390/nano11112856

Ebrahimi, M., Botelho, M. G., & Dorozhkin, S. V. (2017). Biphasic calcium phosphates bioceramics (HA/TCP): Concept, physicochemical properties and the impact of standardization of study protocols in biomaterials research. *Materials Science and Engineering: C Materials for Biological Application*, 71, 1293-1312. https://doi.org/10.1016/j.msec.2016.11.039

Gallant, M. A., Brown, D. M., Hammond, M., Wallace, J. M, Du, J., Deymier-Black, A. C., Almer, J. D., Stock, S. R., Allen, M. R., & Burr, D. B. (2014). Bone cell-independent benefits of raloxifene on the skeleton: a novel mechanism for improving bone material properties. *Bone*, 61, 191-200. https://doi.org/10.1016/j.bone.2014.01.009

Iyyappan, E., Wilson, P., Sheela, K., & Ramya, R. (2016). Role of triton X-100 and hydrothermal treatment on the morphological features of nanoporous hydroxyapatite nanorods. *Materials Science and Engineering: C Materials for Biological Application*, 63, 554-562. https://doi.org/10.1016/j.msec.2016.02.076

Komur, B., Altun, E., Aydogdu, M. O., Bilgiç, D., Gokce, H., Ekren, N., Salman, S., Inan, A. T., Oktarh, F. N., & Gunduz, O. (2017), Hydroxyapatite synthesis from fish bones: Atlantic salmon (Salmon Salar). *Acta Physica Polonica A*, 131(3), 400-402.

Kornphom, C., Saenkam, K., & Bongkarn, T. (2023). Enhanced energy storage properties of BNT–ST–AN relaxor ferroelectric ceramics fabrication by the solid-state combustion technique. *Physica status solidi (a)*, 220(10), Article 2200240. https://doi.org/10.1002/pssa.202200240

Kornphom, C., Saenkam, K., Yotthuan, S., Vittayakorn, N., & Bongkarn, T. (2024). Enhanced electrical and energy storage performances of Fe, Sb co-doped BNBCTS ceramics synthesized via the solid-state combustion technique. *Ceramics International*, 50(23), 51789-51803. https://doi.org/10.1016/j.ceramint.2024.02.203

Kong, Y.-M., Kim, H.-E., Kim, H.-W. (2008). Phase conversion of tricalcium phosphate into Ca-deficient apatite during sintering of hydroxyapatite–tricalcium phosphate biphasic ceramics. *Journal of Biomedical Materials Research Part B*, *Applied Biomaterials*, 84(2), 334-339. https://doi.org/10.1002/jbm.b.30876

Kostov-Kytin, V. V., Dyulgerova, E., Ilieva, R, & Petkova, V., (2018). Powder X-ray diffraction studies of hydroxyapatite and β-TCP mixtures processed by high energy dry milling. *Ceramics International,* 44(7), 8664-8671. https://doi.org/10.1016/j.ceramint.2018.02.094

Koutsopoulos, S. (2002). Synthesis and characterization of hydroxyapatite crystals: a review study on the analytical methods. *Journal of Biomedical Materials Research*, 62(4), 600-612. https://doi.org/10.1002/jbm.10280

Larosi, M. B., Saracho, J. M. P., Pineiro, R. C., Rodriguez, F. L., & Fong, B. M. L. (2009). *Biphasic calcium phosphate and method for obtaining same from fish bones*. EP 2,075,231 A1. European Patent Office.

Latif, A. F. A., Mohd Pu'ad, N. A. S., Ramli, N. A. A., Muhamad, M. S., Abdullah, H. Z., Idris, M. I., & Lee, T. C. (2020). Extraction of biological hydroxyapatite from tuna fish bone for biomedical applications. *Materials Science Forum*, 1010, 584-589. https://doi.org/10.4028/www.scientific.net/msf.1010.584

Lolo, J. A., Ambali, D. P. P., Jefriyanto, W., Handayani, D., Afridah, W., Wikurendra, E. A., Amalia, R., & Syafiuddin, A. (2022). Synthesis and characterization of hydroxyapatite derived from milkfish bone by simple heat treatments. *Biointerface Research in Applied Chemistry*, 12(2), 2440-2449. https://doi.org/10.33263/BRIAC122.24402449

Liou, S.-C., Chen, S.-Y., Lee, H.-Y., & Bow, J.-S. (2004). Structural characterization of nano-sized calcium deficient apatite powders. *Biomaterials*, 25(2), 189-196. https://doi.org/10.1016/S0142-9612(03)00479-4

Malakausaite-Petruleviciene, M., Stankeviciute, Z., Niaura, G., Prichodko, A., & Kareiva, A. (2015). Synthesis and characterization of sol–gel derived calcium hydroxyapatite thin films spin-coated on silicon substrate. *Ceramics International*, 41(6), 7421-7428. https://doi.org/10.1016/j.ceramint.2015.02.055

Motskin, M., Wright, D. M., Muller, K., Kyle, N., Gard, T. G., Porter, A. E., & Skepper, J. N. (2009). Hydroxyapatite nano and microparticles: correlation of particle properties with cytotoxicity and biostability. *Biomaterials*, 30(19), 3307-3317. https://doi.org/10.1016/j.biomaterials.2009.02.044

Muhammad, N., Gonfa, G., Rahim, A., Ahmad, P., Iqbal, F., Sharif, F., Khan, A. S., Khan, F. U., Khan, Z. U. H., Rehman, F., & Rehman, I. U., (2017). Investigation of ionic liquids as a pretreatment solvent for extraction of collagen biopolymer from waste fish scales using COSMO-RS and experiment. *Journal of Molecular Liquids*, 232, 258-264, https://doi.org/10.1016/j.molliq.2017.02.083

Nguyen, T. T. V., Anh, N. P., Ho, T. G.-T., Pham, T. T. P., Nguyen, P. H. D., Do, B. L., Huynh, H. K. P., & Nguyen, T. (2022). Hydroxyapatite derived from salmon bone as green ecoefficient support for ceria-doped nickel catalyst for CO_2 methanation. *ACS Omega,* 7(4), 36623−36633. https://doi.org/10.1021/acsomega.2c04621

Naga, S. M., El-Maghraby, H. F., Mahmoud, E. M., Talaat, M. S., & Ibrhim, A. M. (2015). Preparation and characterization of highly porous ceramic scaffolds based on thermally treated fish bone. *Ceramics International*, 41(10), 15010-15016. https://doi.org/10.1016/j.ceramint.2015.08.057

Onishi, A., Thomas, P. S., Stuart, B. H., Guerbois, J. P., & Forbes, S. L. (2008). TG-MS analysis of the thermal decomposition of pig bone for forensic applications. *Journal of Thermal Analysis and Calorimetry*, 92, 87-90. https://doi.org/10.1007/s10973-007-8741-0

Othman, R., Mustafa, Z., Loon, C. W., & Noor, A. F. M. (2016). Effect of calcium precursors and pH on the precipitation of carbonated hydroxyapatite. *Procedia Chemistry*, 19, 539-545. https://doi.org/10.1016/j.proche.2016.03.050

Permatasari, H. A., Wati, R., Anggraini, R. M., Almukarramah, A., & Yusuf, Y., (2020). Hydroxyapatite extracted from fish bone wastes by heat treatment. *Key Engineering Materials*, 840, 318-323. https://doi.org/10.4028/www.scientific.net/KEM.840.318

Rajesh, R., Hariharasubramanian, A., & Ravichandran, Y. D. (2012). Chicken bone as a bioresource for the bioceramic (hydroxyapatite). *Phosphorus, Sulfur, and Silicon and the Related Elements,* 187(8), 914-925. https://doi.org/10.1080/10426507.2011.650806

Saikumari, N., Dev, S. M., & Dev, S. A. (2021). Effect of calcination temperature on the properties and applications of bio extract mediated titania nano particles. *Scientific Reports*, 11, Article 1734. https://doi.org/10.1038/s41598-021-80997-z

Shi, P., Liu, M., Fan, F., Yu, C., Lu, W., & Du, M. (2018). Characterization of natural hydroxyapatite originated from fish bone and its biocompatibility with osteoblasts. *Materials Science and Engineering C*, 90, 706-712. https://doi.org/10.1016/j.msec.2018.04.026

Suneelkumar, C., Datta, K., Srinivasan, M. R., & Kumar, S. T. (2008). Biphasic calcium phosphate in periapical surgery. *Journal of Conservative Dentistry*, 11(2), 92-96.

Sunil, B. R., & Jagannatham M., (2016). Producing hydroxyapatite from fish bones by heat treatment. *Materials Letters*, 185, 411-414. https://doi.org/10.1016/j.matlet.2016.09.039

Tri, N., Trang, T.N. D., Trinh, N. H. D., Tung, L.T., Van, N.T. T., Anh, N. P., Tan, N. D., No, N. T. H., & Ha, H. K P. (2020). Hydrothermal and calcination regimes and characteristics of nanohydroxyapatite synthesized from *salmon* bones. *Journal of Biochemical Technology,* 11(2), 82-87.

Truite, C. V. R., Noronha, J. N. G., Prado, G. C., Santos, L. N., Palácios, R. S., do Nascimento, A., Volnistem, E. A., Crozatti, T. T. D. S., Francisco, C. P., Sato, F., Weinand, W. R., Hernandes, L., & Matioli, G. (2022). Bioperformance studies of biphasic calcium phosphate scaffolds extracted from fish bones impregnated with free curcumin and complexed with β-cyclodextrin in bone regeneration. *Biomolecules*, 12(3), Article 383. https://doi.org/10.3390/biom12030383

Venkatesan, J., & Kim, S.-K. (2014). Nano-hydroxyapatite composite biomaterials for bone tissue engineering--a review. *Journal of Biomedical Nanotechnology*, 10(10), 3124-3140. https://doi.org/10.1166/jbn.2014.1893

Wang, K., Zhou, C., Hong, Y., & Zhang, X. (2012). A review of protein adsorption on bioceramics. *Interface Focus*, 2(3), 259-277. https://doi.org/10.1098/rsfs.2012.0012

Xu, J. L., Khor, K. A., Dong, Z. L., Gu, Y. W., Kumar, R., & Cheang, P. (2004). Preparation and characterization of nano-sized hydroxyapatite powders produced in a radio frequency (rf) thermal plasma. *Materials Science and Engineering A*, 374(1-2), 101-108. https://doi.org/10.1016/j.msea.2003.12.040

Zhang, Q., Liu, Y., Zhang, Y., Ji, X., Tan, Y., & Liu, Q. (2013). Construction of 3D-ordered hydroxyapatite array structures on Ni foams by Nafion-assisted electrodeposition. *Materials Letters*, 107, 337-339. https://doi.org/10.1016/j.matlet.2013.06.049

Zhu, Q., Ablikim, Z., Chen, T., Cai, Q., Xia, J., Jiang, D., & Wang, S. (2017). The preparation and characterization of HA/β-TCP biphasic ceramics from fish bones. *Ceramics International*, 43(15) 12213-12220. https://doi.org/10.1016/j.ceramint.2017.06.082